

# Suspended Multiwall Carbon Nanotube-Based Infrared Sensors via Roll-to-Roll Fabrication

Jacob John, Martin Muthee, Maruthi Yogeesh, Sigfrid K. Yngvesson, and Kenneth R. Carter\*

Sensors sensitive to infrared radiation based on multiwall carbon nanotubes (MWCNTs) are prepared. The physical suspension and thermal isolation needed for bolometric sensing are achieved by suspending the MWCNTs on polymer gratings fabricated by roll-to-roll (R2R) methods. The physical suspension of MWCNTs on nanoimprinted polymer gratings reduced the thermal link of tubes to the substrate and resulted in an enhanced bolometric photoresponse for the suspended devices. The performance of the R2R fabricated sensor is in the same range as those made by other previously reported wafer batch mode nanofabrication processes and the approximate detectivity of the IR sensor is found to be  $4 \times 10^6 \text{ cm Hz}^{1/2}/\text{W}$ . The successful R2R sensor fabrication process developed in the present work opens up a new low cost, high volume manufacturing technique for the production of sensors based on 1D nanomaterials.

## 1. Introduction

For more than a decade, the unique optoelectronic properties and potential applications of carbon nanotubes (CNTs) have generated widespread scientific interest and its properties as well as electronic structures have been a subject of extensive study. The outstanding photoabsorption in the infrared (IR) spectrum and excellent bolometric characteristics made CNTs promising candidates for IR detector applications.<sup>[1]</sup> Infrared (IR) sensors have numerous applications as they are being used for safety related purposes (flame detection), thermography, night vision, medical imaging, surveillance, industrial process control and in a variety of analytical instruments.<sup>[2]</sup> IR sensors that operate under ambient conditions are becoming the dominating technology for a majority of applications as they are now reaching the performance levels which previously were possible only with cooled IR sensors.

Most of the IR detectors fall into three categories: bolometric, thermoelectric and photovoltaic.<sup>[1,3,4]</sup> Recent work on

thermoelectric<sup>[5,6]</sup> and photovoltaic<sup>[7]</sup> single wall carbon nanotubes (SWCNT) IR detectors shows good performance, but such detectors require asymmetric fabrication processes that are much more complex than what we describe in this paper. Fabrication of bolometric detectors is fairly straightforward and these can conveniently operate at room temperature. The functioning principle behind a bolometric CNT IR sensor involves incident radiation heating the CNT network, resulting in a measurable change in the CNT's electrical resistance since the resistance of CNTs strongly depends on the temperature. Therefore, reducing the CNT film's thermal link to the environment is necessary to obtain an enhanced bolometric

photoresponse.<sup>[1,8]</sup> For efficient bolometer operation, the radiation absorber should have a large absorptivity, low heat capacity, and adequate temperature coefficient of resistance.<sup>[8]</sup> The very low density, high surface area and negligible heat capacity of CNTs make them very responsive as they are very sensitive to incident radiation. Accordingly, little absorption is needed to heat individual nanotubes and give a measurable response. The bolometric detectors require a bias voltage to generate a photoresponse whereas photovoltaic and thermopile detectors can operate under zero voltage.<sup>[6,9]</sup>

CNT-based bolometric IR detectors can be broadly categorized into two groups: i) SWCNT-polymer composite films where SWCNTs are uniformly embedded in polymer matrix<sup>[10–14]</sup> and ii) suspended SWCNT/MWCNT networks or individual bundles prepared by chemical vapor deposition (CVD) or vacuum filtration transfer.<sup>[1,8,15–18]</sup> Recently, the bolometric characteristics of CNT-polystyrene composite films were examined and a responsivity of 500 V/W and response time of around 200 ms for the composite IR sensor were observed.<sup>[12]</sup> Several similar reports on IR sensors based on CNT-polymer composite films show response times on the order of hundreds of milliseconds.<sup>[10–14]</sup> Slower response time and complex sensor fabrication methods unsuitable for large volume fabrication are the major draw backs of CNT-polymer composite IR sensors and printed MWCNT IR sensors<sup>[19]</sup> on plastic. A plastic CNT sensor with the incorporation of an absorber and a reflector for better sensor performance has also been reported.<sup>[20]</sup>

Suspending CNTs in air or vacuum has been shown to reduce their thermal link to the environment leading to significant enhancement of the bolometric photoresponse.<sup>[1,8,15–18]</sup> For example, SWCNT/MWCNT network films were suspended in

Dr. J. John, Prof. K. R. Carter  
Department of Polymer Science and Engineering  
120 Governors Dr, University of Massachusetts  
Amherst, MA 01003, USA  
E-mail: krcarter@polysci.umass.edu  
M. Muthee, M. Yogeesh, Prof. S. K. Yngvesson  
Department of Electrical and Computer Engineering  
130 Natural Resources Rd  
University of Massachusetts  
Amherst, MA 01003, USA



DOI: 10.1002/adom.201400004

vacuum between supporting structures or electrodes that were a few millimeters apart and a dramatic increase in the photoresponse was observed at low temperature with a temperature coefficient of resistance (TCR) of  $\approx 1\% \text{ K}^{-1}$ .<sup>[1]</sup> A suspension of highly aligned MWCNT films was shown to have a responsivity of 30 V/W and a response time of 4.4 ms for the sensor.<sup>[8]</sup> Lu and coworkers reported on the enhanced bolometric response of SWCNT/MWCNT films when they were suspended on lithographically patterned  $\text{SiO}_2 / \text{Si}$  substrates.<sup>[15,16]</sup> The same study indicated that the MWCNTs showed higher sensitivity and faster response than their single wall counterpart when suspended on 500 nm  $\text{SiO}_2$  gratings.

Despite better performance, the fabrication of the aforementioned IR detectors is extremely complex and time consuming, and this remains as a major drawback for this type of IR sensors. For example, the  $\text{SiO}_2 / \text{Si}$  substrate was patterned using e-beam lithography: a tool intensive and time consuming process that makes it challenging to economically fabricate these patterns over larger areas. To complicate matters the SWCNT/MWCNT were deposited using a transfer process where the CNTs are first cast onto a filter membrane by vacuum filtration followed by careful placement and release of this layer on the patterned substrate.<sup>[15,16]</sup> Other techniques used to prepare CNT-based sensor include methods like CVD that require extreme conditions for synthesizing horizontally aligned suspended CNTs<sup>[17,18]</sup> or allowing CNT solutions to slowly evaporate at room temperature for several hours etc.<sup>[21]</sup> All of the above mentioned fabrication processes are time consuming, need extreme conditions, require access to expensive fabrication facilities, and cannot be realistically scaled to large area high throughput fabrication. This lack of a robust and efficient fabrication process is the major disadvantage of almost all of the reported CNT based IR detectors.

We desired to investigate and create a sensitive CNT-based sensor that utilizes a suspended layer of CNTs on sub-micron polymer gratings. Our expertise in roll-to-roll (R2R) nanoimprint lithography (NIL) technique enables the replication of high resolution nanoscale patterns of polymeric nano and micro structures. This patterning can be achieved with enhanced throughput when compared to other advanced patterning techniques such as photolithography and e-beam lithography, etc.<sup>[22–26]</sup> Recently, we demonstrated large-area continuous roll-to-roll nanoimprinting of 1D and 2D micrometer to sub-100 nm features on flexible substrate using perfluoropolyether (PFPE) hybrid molds on a custom designed roll-to-roll nanoimprinter.<sup>[27]</sup> R2RNIL is a platform process technology that can be adapted to a wide range of applications including flat panel displays,<sup>[28,29]</sup> biomedical devices,<sup>[30]</sup> flexible solar cells and antireflective coatings for solar cells.<sup>[31]</sup> But the full potential of R2R NIL fabrication has can be applied to other areas such as the fabrication of physical, chemical and biological sensors etc. R2R fabrication processes—especially in the field of organic electronics—has led to the development of multiple approaches toward electrode deposition, including printing process such as R2R thermal imprinting and silver filling, R2R inkjet printing and R2R flexographic printing.<sup>[32–34]</sup> Although these alternative metal deposition techniques may be suitable for R2R printing electrodes, it was not the focus of our study. Sputter deposition of metal electrodes through a shadow mask

is an established technique and was appropriate for the fabrication of sensors in the present work.

In this article, we utilize high throughput continuous processes to fabricate a new class of MWCNT-based IR detectors that have good responsivity and faster response at room temperature and operate in air provide. This work provides an excellent example of taking advantage of the high-speed R2R nanoimprinting technique and the R2R nanocoating process to provide for potentially low cost, high-speed, large-volume manufacture of multiwall carbon nanotube (MWCNTs) based sensors.

## 2. Results and discussions

**Figure 1** depicts the R2R processes for the fabrication of infrared sensors: a) resist coating, imprinting, and curing, b) nanotube coating, c) electrode deposition. A schematic representation of the R2R fabricated IR sensor is shown in **Figure 1(d)**. Elaborate description of the design and use of the R2R nanoimprinter are described in detail in a previous publication.<sup>[27]</sup> The R2R NanoEmboss 101 tool (Carpe Diem Technologies, MA, USA) consists of five sections, namely unwind, coating, imprinting, metrology/coating, and rewind. A Mayer rod coating technique was used throughout this work. First, a thin layer of polyvinylpyrrolidone (PVP) was coated on the polyethylene terephthalate (PET) substrate to improve photoresist adhesion on PET. A commercially available fast curing photocurable resin, Norland optical adhesive 81 (NOA 81) was used as the imprint resist material in the present work. Accordingly, a 35 wt.% solution of NOA 81 in propylene glycol monomethyl ether acetate (PGMEA) was transferred to the PET substrate and the turning Mayer rod (No. 2.5) removed excess resist material from the substrate. The solvent was fully removed at the drying station (65 °C, dwell time 1 min) in the coating section.

PFPE hybrid molds were placed on a double sided adhesive tape and attached to a rubber cushion layer wrapped around the embossing roller. The molds contained grating patterns having line width 500 nm, same channel spacing and height 500 nm and these patterns were continuously imprinted on to the resist coated on the PET substrate in the embossing section. The resist was able to completely fill the trenches of the nanofeatures and was cured immediately by the UV light (365 nm, 2W). The solidified nanofeatures were continuously peeled off from the embossing roller/R2R mold assembly at a speed of 12 inches per minute. Higher imprint speeds can be realized by either using multiple UV sources or a higher intensity source. A several meter long piece of nanoimprinted web coming out of embossing section is shown in **Figure 2a**.

The patterned substrate was passed under a corona arc surface treatment to improve the wetting properties (**Figure 1b**) and then through the Mayer rod coating station containing a dispersion of MWCNTs in water (3 wt.%). The coating roller deposited an excess of the MWCNT dispersion on the patterned substrate and the Mayer rod (No. 10) removed excess material and provided a uniform coating across the web. The web tension was carefully adjusted to prevent any damage to the nanoscale features on the web during the coating process. The nanotubes coated substrate was then passed through the

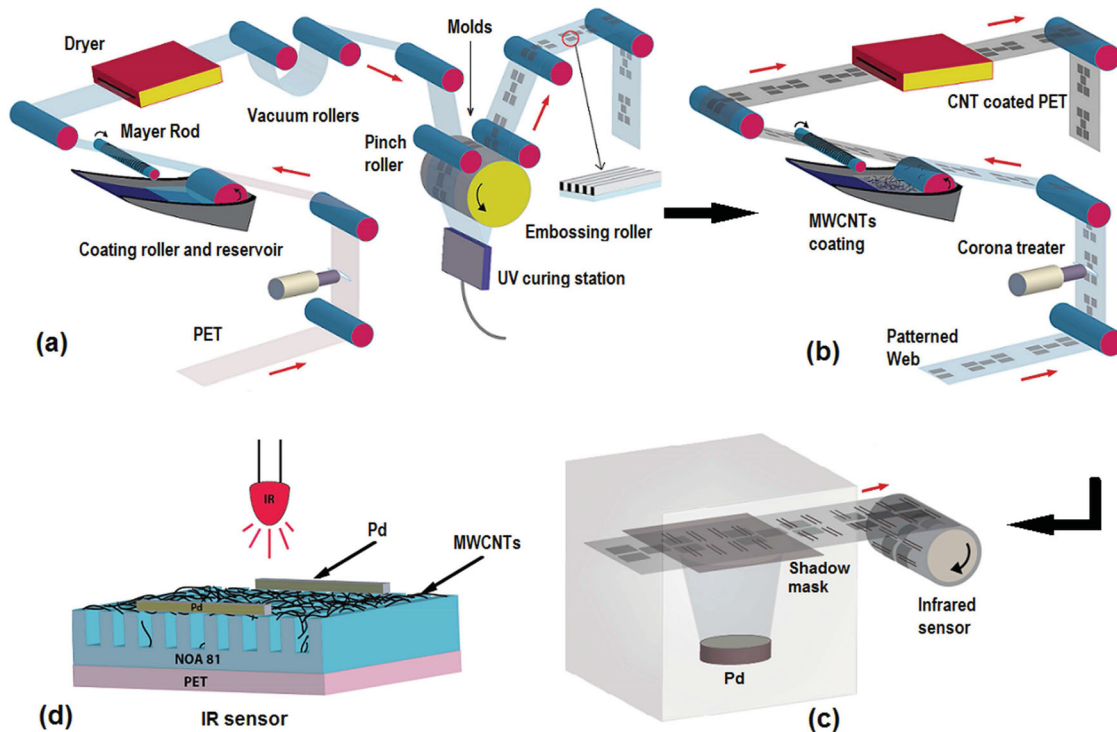


**Figure 1.** R2R processes for the fabrication of infrared sensors: a) R2R coating and nanoimprinting, b) R2R deposition of MWCNTs, c) deposition of electrodes, and d) schematic of a MWCNT-based infrared sensor.

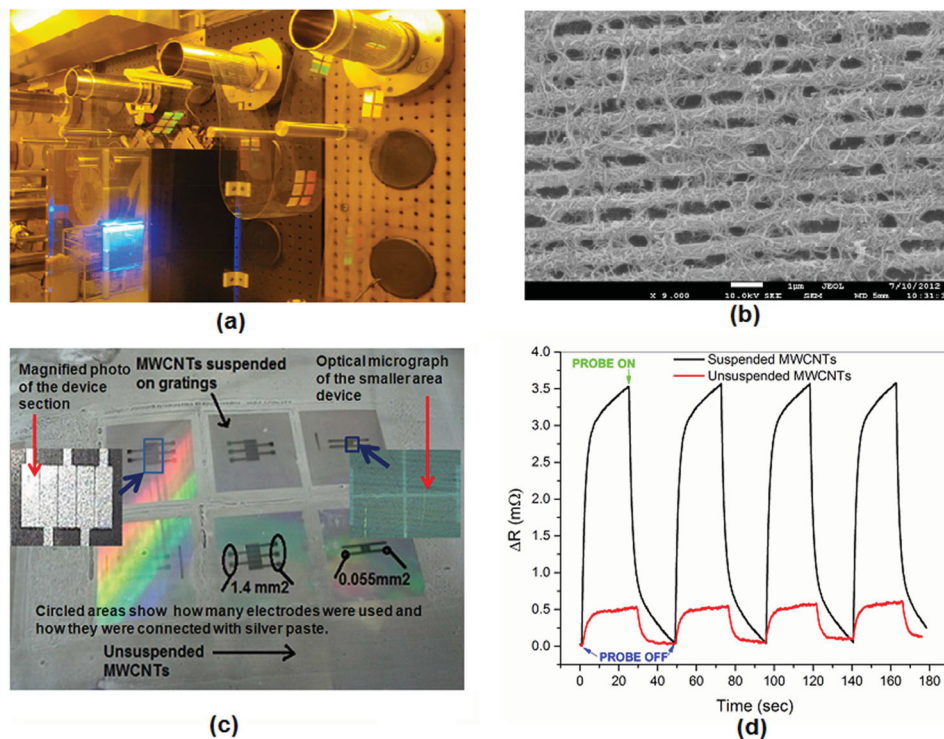


**Figure 2.** a) R2R NIL in process showing several meters of nanoimprinted PET substrate, b) SEM image of suspended MWCNTs on gratings, c) photograph of the R2R fabricated devices showing electrodes used for measurements, and d) photoresponse of suspended and unsuspended MWCNT IR sensors measured at a bias voltage of 400 mV.

drying station (75 °C, dwell time 1 min) to remove the water. Palladium electrodes were sputtered through a shadow mask as shown in Figure 1c which completed the fabrication of the bolometric MWCNT based infrared sensor. Developments in the field of R2R metal evaporation technique make the electrode deposition step R2R compatible as well.<sup>[35]</sup>

The SEM analysis (Figure 2b) revealed a uniform coating of the MWCNTs and the tubes were suspended across the top of the walls of the trenches with little evidence of any tubes entrained within the trenches. Multiwall tubes, being less flexible than their single wall counterparts, increased the probability of suspension after the coating and drying steps. A photograph of the MWCNT IR sensor devices is shown in Figure 2c. There are two different sized devices shown. A larger device (upper left) and a smaller device (upper right), and the dimensions and electrode configurations are shown.

Figure 2a) R2R NIL in process showing several meters of nanoimprinted PET substrate, b) SEM image of suspended MWCNTs on gratings, c) photograph of the R2R fabricated devices showing electrodes used for measurements, and d) photoresponse of suspended and unsuspended MWCNT IR sensors measured at a bias voltage of 400 mV.

The MWCNT film thickness can be varied by changing the concentration of the coating solution, the speed ratio of the coating roller, and using different sized Mayer rods. The thickness of the MWCNT films obtained ranged from 80 to 110 nm. The temperature coefficient of resistance (TCR) of the suspended MWCNT film was measured to be 0.08%/K. The TCR was calculated from the relation (1)

$$TCR = \frac{1}{R} \frac{dR}{dT} \quad (1)$$

The sensor devices were biased at different voltages ranging from 40 mV to 2 V. An IR LED having emission peaked at 940 nm wavelength and output power of 20 mW was used as the IR source and was modulated at regular intervals using a function generator. Changes in electrical resistance ( $\Delta R$ ) of the device was plotted as a function of time when the device was exposed to intermittent IR radiation. As a control, flat devices consisting of unsuspended MWCNTs on PET were also fabricated and the photoresponse of these suspended and unsuspended MWCNT

bolometric sensors and measured at a bias voltage of 400 mV were compared (Figure 2d). A drop in resistance was observed when the IR source was turned on. The initial resistance was fully recovered when the IR source was turned off. The magnitude of the photoresponse of the suspended MWCNT device ( $\Delta R \sim 3.06 \text{ m}\Omega$ ) was found to be almost seven times larger than that of the unsuspended device ( $\Delta R \sim 0.43 \text{ m}\Omega$ ). This dramatic increase of photoresponse demonstrates what can be achieved when the thermal link of MWCNTs with the environment/substrate is minimized by suspending the tubes across the grating gaps. This result supports the argument for a bolometric origin of the photoresponse. The naturally suspended inner CNT shells in multiwall tubes provided an ideal configuration to enhance the bolometric effect by improving light absorption and reducing the thermal link. This ideal configuration makes MWCNTs a better sensing element than their single wall counterpart.<sup>[16]</sup> The physical suspension of MWCNTs on gratings further reduced the thermal link and resulted in an enhanced photoresponse for the suspended devices.

There are two fundamental models proposed for explaining the mechanism of photoresponse of infrared sensitive elements: the interband transition model (band model) and the bolometric model.<sup>[18]</sup> In the interband transition model, the mechanism of the photoresponse is attributed to the photo-excited electrons and holes which enhance the concentration of free carriers and the transport properties of the sensitive elements. In the case of the bolometric model, the energy of the absorbed IR radiation is transferred to the crystal lattice of the sensing elements, thus resulting in an increase in its temperature. The photoresponse in this case comes from the temperature dependence of its resistance. The factors that distinguish the bolometric response from free carrier photoconductivity are: 1) the bolometric response can be reduced by increasing the thermal link between the sensing elements and the environment; 2) the time constant of the bolometric photoresponse is normally 1 to 100 ms; 3) the magnitude of the bolometric response depends on the temperature derivative of the resistance  $dR/dT$ .<sup>[1]</sup> The response time of the MWCNT suspended device taken at 50% magnitude change was in the range of 750–800 ms and is shown in Figure 3a. The longer response time compared with other CNT detectors is likely due to factors such as the large exposure area and thermal conductivity of the

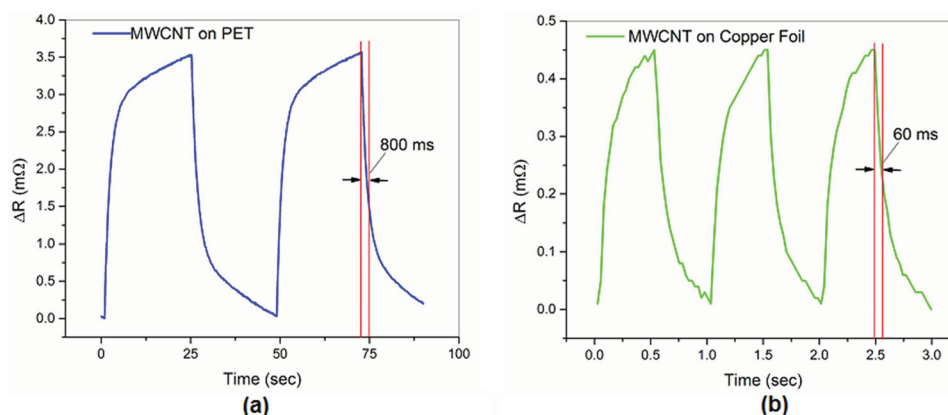


Figure 3. a) Response time measured at 50% magnitude change in signal for suspended IR sensor on PET, b) response time for device on copper.

substrate. Large bolometers are usually very sensitive, but often have a slower response time even though this is not always the case. In this work the exposure area of the devices was  $1.2 \text{ mm}^2$  and was dictated by the shadow mask used to deposit the electrodes. The substrate effect can be understood by considering the thermal time-constant  $\tau$ , which is the ratio of total heat capacity ( $C$ ) of the MWCNT film to the thermal conductance to the surroundings ( $G_{\text{therm}}$ ),

$$\tau = \frac{C}{G_{\text{therm}}} \quad (2)$$

The above relation (2) shows that the thermal conductivity of the substrate can influence the response time.<sup>[36]</sup> The rise in temperature of the MWCNT film upon exposure to IR radiation was calculated using relation (1) and was about 0.3 K. As the MWCNTs were heated by irradiation, there is a three-step process by which the energy is conducted to the environment. Hot electrons in the MWCNTs first relax their energy to the phonons in the MWCNTs. The latter then heat the underlying substrate (resist plus PET or copper) through interface phonon processes. It is assumed that the main path of heat conduction is from the CNTs directly to the substrate, not through the contacts. A detailed analysis of such heat transfer has been performed for the case of single-wall carbon nanotubes (SWCNTs)<sup>[37]</sup> and the same basic steps should apply to MWCNTs, provided that changes are made in some parameters, as explained below. Santavicca and co-workers introduce two possible cases: (1) the acoustic phonon emission process from the electrons to the phonons is limiting; and (2) the process of heat escaping the phonons to the substrate is limiting. In both cases very short energy relaxation times of 6 ps and 300 ps, respectively, are estimated. For MWCNTs no such detailed analysis is available, but a rough estimate can be made. Based on Eq. (2), we use the heat capacity of the MWCNTs instead of SWCNTs and estimate this to be about  $10^3$  times larger. The limiting thermal conductance is likely to be from the phonons to the substrate, as in the case of SWCNTs. Our estimate of the thermal time-constant for the heat transfer from the MWCNTs to the substrate then is about  $10^3$  times that for SWCNTs or 300 ns. Even though this is a rough estimate, we conclude that it is orders-of-magnitude shorter than any of the time-constants we have observed. The “bottle-neck” for transfer of heat from our devices then must be from the substrate to the environment. The thermal conductivity of the photoresist and the PET is much lower than that of inorganic substrates like silicon/ $\text{SiO}_2$  on which CNT bolometric devices have usually been fabricated and this explains the somewhat longer time-constants we measure. By replacing the PET substrate with a higher thermally conductivity substrate, such as metal foil, the response time would be expected to decrease considerably. Accordingly, an infrared sensor of similar device configuration was fabricated using copper foil as the substrate. The resistance vs. time plot of suspended MWCNT on Cu foil device is shown in Figure 3b. As expected, the IR sensor on Cu foil registered a faster detection than the IR sensor on PET. The response time of the Cu device taken at 50% change in resistance was approximately 60 ms as shown in Figure 3b. The shorter thermal path through the photoresist and the higher

thermal conductivity of the Cu foil enabled faster response as expected from the increased  $G_{\text{therm}}$  (expression 2). The performance of an IR sensor can be expressed in terms of the responsivity  $R_v$ , which is defined as the ratio of the output signal generated to the incident power, hence the expression,

$$R_v = \frac{\Delta V}{P_{\text{IR}}} \quad (3)$$

For bolometers,  $R_v$  can also be expressed as (4),

$$R_v = \frac{RI\alpha\eta}{(G_{\text{therm}}^2 + \omega^2 C^2)^{1/2}} \quad (4)$$

where  $R$  is the resistance,  $I$  is the forcing current,  $\alpha$  is the temperature coefficient of the resistance,  $\eta$  is the optical absorption efficiency,  $G_{\text{therm}}$  is the thermal conductance to the heat sink,  $\omega$  is the modulation frequency and  $C$  is the heat capacity of the sensitive element.<sup>[15,36]</sup> Responsivity of the suspended IR sensor on PET was plotted as a function of bias voltage at room temperature and is shown in Figure 4. It can be seen from the plot that higher responsivity was obtained at higher bias voltage, as expected from a bolometric process, while the maximum

$R_v$  obtained for the R2R fabricated MWCNT IR sensor on PET was about 40 V/W. It is also clear that the responsivity of the devices on copper foil should be less based on relation (4). As stated earlier, devices having a smaller exposure area should result in higher responsivity. Accordingly, a suspended MWCNT IR sensor was fabricated on Cu foil substrate having an exposure area of  $0.055 \text{ mm}^2$ . The measured responsivity of the sensor at a bias voltage of 2.5 V was found to be 110 V/W. This is much higher than the responsivity of the Cu foil device with larger exposure area ( $1.4 \text{ mm}^2$ ) which was about 8 V/W. The larger responsivity for the smaller device agrees with the relation (4) since  $G_{\text{therm}}$  is proportional to the area. The detectivity,  $D^*$  can be calculated from the expression (5),

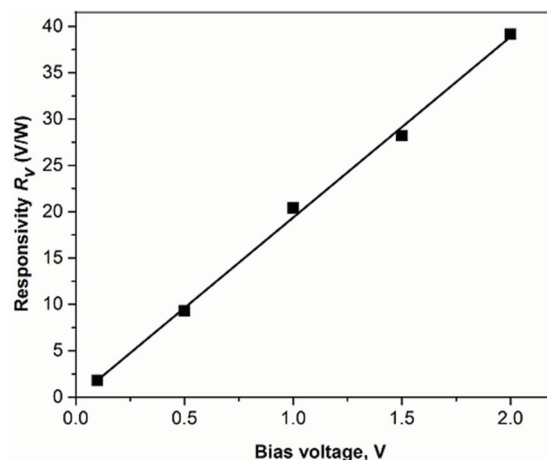


Figure 4. Responsivity of the R2R IR sensor on PET at different bias voltages.

$$D^* = \frac{R_v \sqrt{A_d}}{V_n} \quad (5)$$

in which  $A_d$  is the active area of detector and  $V_n$  is the root mean square noise voltage per unit band width.<sup>[15,36]</sup> We estimated the noise voltage in a 1 Hz bandwidth as  $\Delta R^* I$  (bias voltage, 400 mV) from recordings such as Figure 3 by expanding the vertical scale. Here,  $I$  is the bias current. No audio spectrum analyzer was available, so the spectral dependence of the noise is not known. The temperature dependence of the noise voltage should be negligible since the temperature change estimated above is negligible. Our approximate estimate of the detectivity of the R2R MWCNT IR sensor is  $4 \times 10^6 \text{ cm Hz}^{1/2} / \text{W}$ . The responsivity and response time of the new R2R MWCNT IR sensors are in the same range as most of the CNT-based sensor devices made by classic wafer-based processes found in earlier reports.<sup>[1,4,8,10–18]</sup> Most importantly, the fabrication steps for all previous MWCNT IR detectors involved tedious procedures that cannot be realized on a continuous high-speed and low cost process platform. Higher responsivities and faster response in R2R MWCNT sensors can be achieved by reducing the exposure area and using a substrate with higher thermal conductivity.

### 3. Conclusions

We developed and successfully implemented a novel R2R sensor fabrication technique for the high-throughput manufacturing of a highly sensitive, low cost infrared sensor based on suspended MWCNTs. This was accomplished by taking advantage of a R2R nanoimprinting technique and a simple R2R nanocoating process which allows for the fabrication of hundreds of devices on PET films in a short period of time. The physical suspension of MWCNTs on R2R nanoimprinted polymer gratings reduced the thermal link of tubes to the surroundings and resulted in an enhanced bolometric photoresponse for the suspended devices. The performance of the R2R fabricated sensor was in the same range as those in earlier reports and the approximate detectivity of the IR sensor was found to be  $4 \times 10^6 \text{ cm Hz}^{1/2} / \text{W}$ . A number of other substrates can also be used in place of PET such as metal foils, papers and fabrics depending on the process conditions and applications. This new methodology will substantially bring down the cost of sensors. The novel roll-to-roll sensor fabrication technique outlined in this work opens a new pathway for the fabrication of physical, chemical, biological, and environmental sensors based on 1D nanomaterials like nanowires,<sup>[38]</sup> nanofibers,<sup>[39,40]</sup> and functionalized nanotubes<sup>[41]</sup> etc.

### 4. Experimental Section

**Materials:** Polyethylene terephthalate (PET) roll (ST 505, 125  $\mu\text{m}$  thick, DuPont) was purchased from Tekra Corporation, WI, USA. Polyvinylpyrrolidone (PVP-K30) was purchased from ISP Technologies, INC, NJ, USA. Norland Optical Adhesives 81 and 74 were purchased from Norland Products, NJ, USA. Multiwall carbon nanotube dispersion (3 wt.%) in DI water was purchased from US Nanomaterials, INC, USA

and was used as received. Nanotube specifications: OD 50–80 nm and L 10–20  $\mu\text{m}$ . Perfluoropolyether acrylate (CN4002) was purchased from Sartomer USA, LLC. Vertral XF (DuPont) solvent was supplied by Cornerstone Technology, Inc. Benzoin methyl ether, propylene glycol monomethyl ether acetate (PGMEA) and 2-butanol were purchased from Sigma-Aldrich Company and were used as received.

**Instrumentation/Sensor Testing:** The description and use of a custom designed R2R NanoEmboss 101 R2R nanoimprinter was reported in an earlier article.<sup>[27]</sup> SEM images were taken using JEOL JSM – 7001F SEM. The palladium electrodes were deposited using shadow masks in an AJA International Orion 8 sputtering system. All the fabricated sensors were tested using a Keithley 2600 source meter. The infrared LED (peak emission at 940 nm) was modulated using an HP 8116A pulse/function generator. The output power of the IR source was measured using a Scientech Astral AA30 power meter and was found to be 20 mW. The electrodes used for measurements and their dimensions are marked in Figure 2c. A magnified image of the large area device and an optical image of the smaller device are shown in the image. For the measurement using larger device, we used all 5 electrodes. The gap between electrodes is 100  $\mu\text{m}$  and the total area is 1.4  $\text{mm}^2$ . In the case of smaller device, we used only two electrodes out of the four during the detection measurement. The gap between the electrodes is 50  $\mu\text{m}$  and the total exposure area is 0.055  $\text{mm}^2$ .

**Fabrication of the PFPE Acrylate Hybrid Mold:** The PFPE acrylate (CN4002) was mixed with photoinitiator benzoin methyl ether (BME) (2 wt%) using Vertral XF as the solvent for 1 hour. A plasma treated PET sheet was spin coated with a thin layer of NOA 74 (as an adhesion promoter) and thereafter cured under UV light ( $\lambda$  365 nm) for 3 minutes. The fluoroacrylate solution was spin coated on the Si master mold (1000 rpm, 45 sec). The PET with cured NOA 74 layer was placed on top of the fluoroacrylate coated Si master with the adhesive layer facing the master mold and the entire assembly was placed in the Nanonex Nanoimprinter (NX 2000) for UV curing ( $\lambda$  = 365 nm) under nitrogen atmosphere for 20 minutes. The PET supported replica was manually peeled from the silicon master and the patterned crosslinked PFPE acrylate remained adhered to the PET backing layer.

**Roll-to-Roll Nanocoating:** In order to improve the wetting properties of the resist and enhance adhesion to the PET substrate, we coated the substrate with 1 wt.% solution of polyvinylpyrrolidone (PVP) in 2-butanol using a Mayer rod (No. 4) coating station, dried and rewound on to the rewind roller with an interleaf. A 35 wt.% solution of NOA 81 in propylene glycol monomethyl ether acetate (PGMEA) was used as coating solution for resist coating. The MWCNTs were coated using a 3 wt.% solution of MWCNT dispersion in DI water. The corona surface treatment (BD-20AC Corona treater) was applied to the R2R imprinted substrate while it was fed to the coating station for nanotube coating. The speed ratio of the coating roller was kept at one and the web speed was synchronized with the speed of the embossing roller. The Mayer rod (no. 2.5 and 10) rotation was kept at 10 rpm throughout the entire process. The solvents were removed at the drying station above the coating unit.

**Roll-to-Roll Nanoimprinting:** An array of PFPE hybrid molds were attached to a double-sided tape and wrapped around the embossing roller having 6 inches in diameter and width. A rubber cushion layer was placed between the roller and the mold to ensure conformal contact during the process. When the resist coated web was fed into the embossing roller, the two vacuum rollers on either side of the embossing roller applied web tension and the pinch roller pressed the coated web against the roll-to-roll mold assembly on the embossing roller. The resist was cured by the UV light source (Omnigure 1000, EXFO) placed at 5 to 7 mm distance from the embossing roller and operating at 90% iris opening (2 W,  $\lambda$  = 365 nm). The web speed was maintained between 10 to 14 inches per minute. The cured resist and web were continuously separated from the mold at the release roller as the web moved forward.

**Temperature Coefficient of Resistance (TCR) Measurement:** The temperature coefficient of resistance of MWCNTs was measured by monitoring the change in resistance with temperature using a hot plate with precise temperature control. The detectors were placed in good

thermal contact with this hotplate. The measurements were taken at every 5 degree increment starting from room temperature (293 K) to 348 K. The data was collected after the device was allowed to remain at the set temperature for almost 15 minutes.

## Acknowledgements

This work was financially supported by the NSF Nanoscale Science and Engineering Center for Hierarchical Manufacturing (CHM) at the University of Massachusetts – Amherst, MA 01003, USA (Grant No: CMMI-1025020). We also thank the Panasonic Boston Research Laboratory for kind support. Authors thank John Berg, CEO, Carpe Diem Technologies, Franklin, MA, USA for his assistance in designing and building the R2R NanoEmboss 100 nanoimprinter. John Nicholson of Conte Nanotechnology cleanroom lab (CHM) at PSE, UMASS, Amherst is also acknowledged for providing assistance with characterization facilities.

Received: January 6, 2014

Revised: February 10, 2014

Published online:

- [1] M. E. Itkis, F. Borondics, A. Yu, R. C. Haddon, *Science* **2006**, 312, 413.
- [2] F. Niklaus, C. Vieider, H. Jakobsen, *Proc. SPIE, MEMS/MOEMS Technologies and Applications III* **2007**, 6836, 68360D D1.
- [3] L. Yang, S. Wang, Q. Zeng, Z. Zhang, L.-M. Peng, *Small* **2013**, 9, 1225.
- [4] M. Tarasov, J. Svensson, L. Kuzmin, E. E. B. Campbell, *Appl. Phys. Lett.* **2007**, 90, 163503.
- [5] X. He, X. Wang, S. Nanot, K. Cong, Q. Jiang, A. A. Kane, J. E. M. Goldsmith, R. H. Hauge, F. Léonard, J. Kono, *ACS Nano* **2013**, 7, 7271.
- [6] B. C. St-Antoine, D. Ménard, R. Martel, *Nano Lett.* **2010**, 11, 609.
- [7] Q. Zeng, S. Wang, L. Yang, Z. Wang, T. Pei, Z. Zhang, L.-M. Peng, W. Zhou, J. Liu, W. Zhou, S. Xie, *Opt. Mater. Exp.* **2012**, 2, 839.
- [8] L. Xiao, Y. Zhang, Y. Wang, K. Liu, Z. Wang, T. Li, Z. Jiang, J. Shi, L. Liu, Q. Li, Y. Zhao, Z. Feng, S. Fan, K. Jiang, *Nanotechnology* **2011**, 22, 025502.
- [9] L. J. Yang, S. Wang, Q. S. Zeng, Z. Y. Zhang, L. M. Peng, *Small* **2013**, 9, 1225.
- [10] A. E. Aliev, *Infrared Phys. Technol.* **2008**, 51, 541.
- [11] D. Bang, J. Lee, J. Park, J. Choi, Y. W. Chang, K.-H. Yoo, Y.-M. Huh, S. Haam, *J. Mater. Chem.* **2012**, 22, 3215.
- [12] A. Y. Glamazda, V. A. Karachevtsev, W. B. Euler, I. A. Levitsky, *Adv. Funct. Mater.* **2012**, 22, 2177.
- [13] B. Pradhan, R. R. Kohlmeier, K. Setyowati, H. A. Owen, J. Chen, *Carbon* **2009**, 47, 1686.
- [14] B. Pradhan, K. Setyowati, H. Liu, D. H. Waldeck, J. Chen, *Nano Lett.* **2008**, 8, 1142.
- [15] R. Lu, Z. Li, G. Xu, J. Z. Wu, *Appl. Phys. Lett.* **2009**, 94, 163110.
- [16] R. Lu, J. J. Shi, F. J. Baca, J. Z. Wu, *J. Appl. Phys.* **2010**, 108, 84305.
- [17] M. Mahjour-Samani, Y. S. Zhou, X. N. He, W. Xiong, P. Hilger, Y. F. Lu, *Nanotechnology* **2013**, 24, 035502.
- [18] F. Rao, X. Liu, T. Li, Y. Zhou, Y. Wang, *Nanotechnology* **2009**, 20, 055501.
- [19] A. Gohier, A. Dhar, L. Gorintin, P. Bondavalli, Y. Bonnassieux, C. S. Cojocaru, *Appl. Phys. Lett.* **2011**, 98, 63103.
- [20] K. Narita, R. Kuribayashi, E. Altintas, H. Someya, K. Tsuda, K. Ohashi, T. Tabuchi, S. Okubo, M. Imazato, S. Komatsubara, *Sens. Actuat. A* **2013**, 195, 142.
- [21] G. Vera-Reveles, T. J. Simmons, M. Bravo-Sanchez, M. A. Vidal, H. Navarro-Contreras, F. J. Gonzalez, *ACS Appl. Mater. Inter.* **2011**, 3, 3200.
- [22] S. H. Ahn, L. J. Guo, *Adv. Mater.* **2008**, 20, 2044.
- [23] S. H. Ahn, L. J. Guo, *ACS Nano* **2009**, 3, 2304.
- [24] E. A. Costner, M. W. Lin, W.-L. Jen, C. G. Willson, *Annu. Rev. Mater. Res.* **2009**, 39, 155.
- [25] L. J. Guo, *Adv. Mater.* **2007**, 19, 495.
- [26] N. R. Hendricks, K. R. Carter, in *Comprehensive Polymer Science*, 2nd Ed, Elsevier, **2012**, p. 251.
- [27] J. John, Y. Tang, J. P. Rothstein, J. J. Watkins, K. R. Carter, *Nanotechnology* **2013**, 24, 505307.
- [28] A. Jeans, M. Almanza-Workman, R. Cobene, R. Elder, R. Garcia, F. Gomez-Pancorbo, W. Jackson, M. Jam, H.-J. Kim, O. Kwon, H. Luo, J. Maltabes, P. Mei, C. Perlov, M. Smith, C. Taussig, F. Jeffrey, S. Braymen, J. Hauschildt, k. Junge, D. Larson, D. Stieler, *Proc. SPIE, Alternative Lithographic Technologies II* **2010**, 7637, 763719.
- [29] H.-J. Kim, M. Almanza-Workman, B. Garcia, O. Kwon, F. Jeffrey, S. Braymen, J. Hauschildt, K. Junge, D. Larson, D. Stieler, A. Chaiken, B. Cobene, R. Elder, W. Jackson, M. Jam, A. Jeans, H. Luo, P. Mei, C. Perlov, C. Taussig, *J. Soc. Information Display* **2009**, 17, 963.
- [30] A. L. Vig, T. Makela, P. Majander, V. Lambertini, J. Ahopelto, A. Kristensen, *J. Micromech. Microeng.* **2011**, 21, 035006.
- [31] M. A. G. Lazo, R. Teuscher, Y. Leterrier, J. E. Månson, C. Calderone, A. Hessler-Wyser, P. Couty, Y. Ziegler, D. Fischer, *Sol. Energy Mater. Sol. Cells* **2012**, 103, 147.
- [32] J. Jensen, M. Hösel, I. Kim, J.-S. Yu, J. Jo, F. C. Krebs, *Adv. Funct. Mater.* **2013**, DOI:10.1002/adfm.201302320.
- [33] R. R. Søndergaard, M. Hösel, F. C. Krebs, *J. Poly. Sci. B: Polymer Physics* **2013**, 51, 16.
- [34] J.-S. Yu, I. Kim, J.-S. Kim, J. Jo, T. T. Larsen-Olsen, R. R. Søndergaard, M. Hosel, D. Angmo, M. Jorgensen, F. C. Krebs, *Nanoscale* **2012**, 4, 6032.
- [35] C. F. Struller, P. J. Kelly, N. J. Copeland, C. M. Liauw, *J. Vac. Sci. Tech. A: Vacuum, Surfaces, and Films* **2012**, 30, 041502.
- [36] P. Renoux, S. A. Jonsson, L. J. Klein, H. F. Hamann, S. Ingvarsson, *Optics Express* **2011**, 19, 8721.
- [37] D. F. Santavica, J. D. Chudow, D. E. Prober, M. S. Purewal, P. Kim, *Nano Lett.* **2010**, 10, 4538.
- [38] N. S. Ramgir, Y. Yang, M. Zacharias, *Small* **2010**, 6, 1705.
- [39] C. Burger, B. S. Hsiao, B. Chu, *Annu. Rev. Mater. Res.* **2006**, 36, 333.
- [40] Q. Gao, H. Meguro, S. Okamoto, M. Kimura, *Langmuir* **2012**, 28, 17593.
- [41] C. Gao, Z. Guo, J. H. Liu, X. J. Huang, *Nanoscale* **2012**, 4, 1948.